Two-neutrino double-β decay matrix elements based on a relativistic nuclear energy density functional

Popara, N.; Ravlić, A.; Paar, N.

Two-neutrino double-β decay matrix elements based on a relativistic nuclear energy density functional

N. Popara [*]
Faculty of Veterinary Medicine, University of Zagreb, Heinzelova c. 102, 10000 Zagreb, Croatia
and Department of Physics, Faculty of Science, University of Zagreb, Bijenička c. 32, 10000 Zagreb, Croatia

A. Ravlić [†] and N. Paar [‡]
Department of Physics, Faculty of Science, University of Zagreb, Bijenička c. 32, 10000 Zagreb, Croatia

(Received 3 September 2020; revised 19 July 2021; accepted 19 May 2022; published 24 June 2022)

Nuclear matrix elements (NMEs) for two-neutrino double-β decay ($2\nu\beta\beta$) are studied in the framework of a relativistic nuclear energy density functional. The properties of nuclei involved in the decay are obtained using the relativistic Hartree-Bardeen-Cooper-Schrieffer theory and relevant nuclear transitions are described using the relativistic proton-neutron quasiparticle random phase approximation based on the relativistic energy density functional. Three effective interactions are employed, including density-dependent meson-exchange (DD-ME2) and point-coupling interactions (DD-PC1 and DD-PCX), and pairing correlations are described consistently both in $T = 1$ and $T = 0$ channels using a separable pairing interaction. The optimal values of $T = 0$ pairing strength parameter V_{0pp} are constrained by the experimental data on β-decay half-lives. The $2\nu\beta\beta$ matrix elements and half-lives are calculated for several nuclides experimentally known to undergo this kind of decay: ^{48}Ca, ^{76}Ge, ^{82}Se, ^{96}Zr, ^{100}Mo, ^{116}Cd, ^{124}Xe, ^{128}Te, ^{130}Te, ^{136}Xe, and ^{150}Nd. The model dependence of the NMEs and their sensitivity on V_{0pp} is investigated, and the NMEs obtained using optimal values of V_{0pp} are discussed in comparison to previous studies. The results of the present work represent an important benchmark for the future applications of the relativistic framework in studies of neutrinoless double-β decay.

DOI: 10.1103/PhysRevC.105.064315

I. INTRODUCTION

The study of double-β decays has attracted considerable interest over the past years [1,2]. Most of this interest has been focused on the neutrinoless mode ($0\nu\beta\beta$), because it offers the possibility of distinguishing between the Dirac and Majorana nature of neutrinos [3]. The two-neutrino double-β decay mode ($2\nu\beta\beta$), nonetheless, remains of interest as an important benchmark of theoretical models for further studies of ($0\nu\beta\beta$) decays. The $2\nu\beta\beta$ decay is a second-order weak interaction process, and as such it is allowed by the standard model [4], unlike the neutrinoless mode, which violates lepton conservation and consequently requires physics beyond the standard model [5]. Furthermore, it is possible to experimentally observe this mode, as pairing in even-even nuclei makes them more stable than adjacent odd-odd nuclei, and the transition from an even-even mother to an odd-odd daughter is forbidden energetically, leaving double-β decay as the only allowed decay channel [6]. This allows us to compare the results of our calculations to experiment directly, and, since the calculations for the neutrinoless mode use the same ingredients as those for the two-neutrino mode, their results can be used to constrain some of the model parameters and benchmark the model for studies of $0\nu\beta\beta$ decay [7].

The contribution of nuclear physics to the calculation of decay rates for both modes of double-β decay is contained chiefly in the nuclear matrix element (NME) [8]. A variety of theoretical approaches has been developed in the past years for the description of double-β decay NMEs. More detailed information is available in the following extensive reviews [2,6,9–18]. The calculations of NMEs have been carried out using various approximations: the quasiparticle random phase approximation (QRPA) [19–21], its extension to the renormalized QRPA (RQRPA) [22–25], the second QRPA (SQRPA) [26,27], various energy density functional (EDF) approaches [28,29], the quasiparticle Tamm-Dancoff approximation [30], the interacting shell model (ISM) and similar approaches [31–33], the interacting boson model (IBM) [34–37], and others [38–40]. Among these approximations, the proton-neutron quasiparticle random-phase approximation (pn-QRPA) has emerged as one of the approaches that has been successfully employed in various studies of double-β decays [1,41–43]. Within this approach, the usual isovector pairing in the ground state of open-shell nuclei is supplemented with an isoscalar proton-neutron pairing in the residual interaction. This has been shown to be important in nuclei relevant for double-β decays (as first established by Refs. [44,45] and confirmed by subsequent studies [46,47], including work beyond the

[*] nato.popara@vef.unizg.hr
[†] aravlic@phy.hr
[‡] npaar@phy.hr

QRPA [48,49]). In the relativistic framework, various methods have been employed in studies of $0\nu\beta\beta$ decays. In Ref. [50] a multireference covariant EDF was used to determine the wave functions of the initial and final nuclei, and correlations beyond the mean field were described by configuration mixing of both angular momentum and particle number projected quadrupole deformed mean-field wave functions. Systematic study of $0\nu\beta\beta$ matrix elements in the relativistic EDF approach was reported in Ref. [51], and effects of the relativity and short-range correlations have recently been analyzed [52].

The aim of this work is to establish a theory framework for the description of $2\nu\beta\beta$ decay NMEs based on a modern relativistic nuclear energy density functional with density-dependent point-coupling and meson-exchange interactions that include density dependence explicitly in the interaction vertex functions. These interactions were recently introduced and successfully implemented in the description of nuclear excitation properties [53–58], astrophysically relevant weak interaction processes [59–62], and nuclear equation of state [63–65]. In previous relativistic EDF studies $2\nu\beta\beta$ decays have not been addressed [50–52]. We note that the present theory framework includes the density dependence explicitly in the vertex functions of the meson-exchange and point-coupling interactions.

When modeling various quantities in nuclear physics, it is important to assess systematic errors. As pointed out in Ref. [66] the systematic error of a theoretical model may be a consequence of missing physics and/or poor modeling. Considering that in most cases the perfect model is not available, systematic errors are rather difficult to estimate. However, some insight about systematic uncertainties can be obtained from a comparative study of different theory frameworks and effective nuclear interactions. Therefore, it is important to address the problem of double-β decays both from nonrelativistic and relativistic frameworks, using various formulations of energy density functionals and different parametrizations.

Since for the $2\nu\beta\beta$ decay mode experimental data exist for a set of nuclei, the present study also allows us to benchmark the relativistic model for the future studies of $0\nu\beta\beta$ decay. The properties of nuclei involved are described using the relativistic Hartree-Bardeen-Cooper-Schrieffer (RH-BCS) model, while relevant transitions are obtained using the proton-neutron relativistic quasiparticle random phase approximation [67], which was recently extended by including relativistic density-dependent point-coupling interactions [68,69]. In the following we denote this method as REDF-QRPA. Model calculations of the NMEs include various double-β emitters: ^{48}Ca, ^{76}Ge, ^{82}Se, ^{96}Zr, ^{100}Mo, ^{116}Cd, ^{124}Xe, ^{128}Te, ^{130}Te, ^{136}Xe, and ^{150}Nd. In contrast to recent studies based on the pn-QRPA, which tend to start from a "realistic" nucleon-nucleon interaction [70,71], in the present work in the particle-hole channel we use an interaction derived from a relativistic nuclear energy density functional. An important aspect of this study is that we are able to explore the model dependence of the calculated NMEs, by implementing two different types of relativistic density-dependent interactions, (i) finite range meson-exchange and (ii) point-coupling interactions. Our model calculations also involve a treatment of the pairing correlations in open-shell nuclei, both at the level of the nuclear ground state and in the residual REDF-QRPA interaction. In particular, strength of the proton-neutron pairing, that is, isoscalar $T = 0$ pairing in the residual REDF-QRPA interaction, has to be constrained by using experimental data, in a similar way as already discussed in previous studies in nonrelativistic frameworks [7]. In the present study the experimental data on single-β decays will be employed to constrain the $T = 0$ pairing strength parameter for applications in $2\nu\beta\beta$ and in intended future $0\nu\beta\beta$ matrix element calculations.

We note that in this work, which represents the first implementation of the relativistic density-dependent interactions in $2\nu\beta\beta$ decay study, some effects have not yet been taken into account, from deformation [72,73] to renormalization and gauge symmetry [74] and isospin restoration [75,76]. In forthcoming studies more advanced effects will be taken into account. Nonetheless, we expect that the present work will describe well at least some subset of the double-β emitters, and will provide a useful guidance for the future studies.

This article is organized as follows: in Sec. II we provide a theoretical overview concerning the matrix elements involved in double-β decay and in Sec. III we outline the relativistic theory framework. Results are provided and discussed in Sec. IV, and the conclusion follows in Sec. V.

II. TWO-NEUTRINO DOUBLE-β DECAY

Two-neutrino double-β decay ($2\nu\beta\beta$) is the process whereby two neutrons in the mother nucleus are converted into protons, accompanied by the emission of two electrons and two antineutrinos:

$$(A, Z) \rightarrow (A, Z + 2) + 2e^- + 2\bar{\nu}. \tag{1}$$

The half-life of two-neutrino double-β decay formally depends on two matrix elements [77],

$$\frac{1}{T^{2\nu}_{1/2}} = G^{2\nu}(Q, Z) g_A^4 \left[\mathcal{M}^{2\nu}_{GT} + \mathcal{M}^{2\nu}_{F}\right]^2, \tag{2}$$

where $\mathcal{M}^{2\nu}_{GT}$ and $\mathcal{M}^{2\nu}_{F}$ are, respectively, the Gamow-Teller (GT) and Fermi matrix element, and $G^{2\nu}(Q, Z)$ is a phase space factor that can be found tabulated, e.g., in Ref. [78]. The factor g_A is the axial-vector coupling constant.

We restrict our consideration to decays from a 0^+ state to a 0^+ state. Decays to the states of higher angular momenta, e.g., 2^+, are possible, albeit highly suppressed. Their treatment would require a computational apparatus more involved than the REDF-QRPA used in this work [79]. The Gamow-Teller matrix element in this case can be written as [18]

$$\mathcal{M}^{2\nu}_{GT} = m_e \sum_m \frac{\langle f | \sum_a \sigma_a \tau^-_a | m \rangle \langle m | \sum_a \sigma_a \tau^-_a | i \rangle}{E_m + \frac{Q}{2} + m_e}, \tag{3}$$

where the sum goes over 1^+ states in the intermediate nucleus, labeled with m and having the energy E_m as measured from the ground state of the initial nucleus. The Q value of the double-β decay reads

$$Q = (m_i - m_f)c^2 - 2m_e. \tag{4}$$

Note that we could have also chosen to group the factor g_A^2 into the definition of the matrix element in Eq. (3), in order to make the discussion about the effects of g_A and its renormalization easier. If the two are grouped together, one obtains an effective NME $M^{2\nu}_{GT,\mathrm{eff}}$ that depends on the choice of the axial-vector coupling as well [80]. In this work, instead of the free nucleon value $g_A = 1.26$, we employ a quenched value $g_A = 1.0$ that is consistent with the previous REDF-QRPA studies of β-decay half-lives as well as electron capture rates [81–83]. Thus our results for the matrix elements in Eq. (3) can be directly compared with those of the effective NMEs from Ref. [80]. Likewise, we introduce the factor m_e (in MeV) in the definition of the nuclear matrix element to obtain dimensionless NMEs that can be compared easily to results of recent theoretical and experimental works. Otherwise, the matrix elements would be in units of MeV^{-1}. In all figures and tables in this work, the REDF-QRPA results for $M^{2\nu}_{GT}$ and $M^{2\nu}_{GT,\mathrm{eff}}$ are given as dimensionless.

The closure approximation is widely used in calculating $2\nu\beta\beta$ decay. It entails the replacement of the sum over different states in the intermediary nucleus, as in Eq. (3), with a form that consists of one denominator containing a suitably chosen "average" energy $\langle E\rangle$:

$$\mathcal{M}^{2\nu}_{GT,\mathrm{closure}} = m_e \frac{\langle f|\sum_a \sigma_a \tau_a^- \sum_a \sigma_a \tau_a^- |i\rangle}{\langle E\rangle + \frac{Q}{2} + m_e}. \tag{5}$$

In this work we calculate the NMEs using the more complete approach given in Eq. (3), but where relevant for the comparison with other studies we include the closure approximation as well. It can be shown that the Fermi matrix element vanishes if the same pairing interaction is consistently used at both the ground state and excitation levels in the isovector channel [84]. This is the case for our calculation and as such we will not show the Fermi matrix element. The REDF-QRPA is not applicable to transitions from the 1^+ intermediate nucleus. Therefore, although we conceive of double-β decay as a sequence of two β^+, β^-, or electron capture decays [85], in the present study we calculate β^- decay from the initial 0^+ nucleus and a β^+ decay from the final 0^+ nucleus, resulting in two sets of intermediate 1^+ states. Explicitly, for the GT transitions the matrix element is given by

$$\mathcal{M}^{2\nu}_{GT} = m_e \sum_{m'm} \frac{\langle m|\sum_a \sigma_a \tau_a^- |i\rangle \langle m|m'\rangle \langle f|\sum_a \sigma_a \tau_a^- |m'\rangle}{E_m + \frac{Q}{2} + m_e}. \tag{6}$$

For the overlap between states belonging to different sets we take the usual prescription [41]:

$$\langle m|m'\rangle \approx \sum_{pn} \left[X^m_{pn} X^{m'}_{pn} - Y^m_{pn} Y^{m'}_{pn}\right], \tag{7}$$

where the quantities X and Y are the REDF-QRPA amplitudes that will be defined in the next section. This is an approximation in cases where the initial and final states are not identical, but a reasonable one. For ^{48}Ca, for example, we calculate the overlap between the lowest states belonging to each of the different sets of states in the intermediate nucleus to be 0.9855. Higher states in one set are more likely to have significant overlap with several states in the other, but the values of the overlaps still go from around 0.14 toward higher ones around 0.89. An alternative prescription from Šimkovic *et al.* [41] involves additional factors proportional to occupation numbers:

$$\langle m|m'\rangle \approx \sum_{pn} \left[X^m_{pn} X^{m'}_{pn} - Y^m_{pn} Y^{m'}_{pn}\right] \tilde{u}_p \tilde{u}_n, \tag{8}$$

where the quantities $\tilde{u}_{p/n}$ are defined as follows:

$$\tilde{u}_{p/n} = u^m_{p/n} u^{m'}_{p/n} + v^m_{p/n} v^{m'}_{p/n}, \tag{9}$$

and $u_{p/n}$, $v_{p/n}$ are occupation numbers derived, in the present work, from the relativistic Hartree-BCS model (more details are given in Sec. III). Several effects are usually neglected in the study of $2\nu\beta\beta$ decays, such as higher-order currents and realistic short-range correlations [86], that are important in the neutrinoless case. This is due to the insensitivity of the two-neutrino NMEs to the details of the nucleon wave functions for low nucleon separation r_{12} [86].

III. RELATIVISTIC FRAMEWORK FOR $2\nu\beta\beta$ DECAY MATRIX ELEMENTS

A. Relativistic Hartree-BCS for the ground-state description

Calculations of nuclear matrix elements for double-β decay often proceed starting from a realistic nucleon-nucleon potential [16,87]. As mentioned in Sec. I, other theory frameworks based on phenomenological effective interactions have also been employed, in particular the shell model and nuclear energy density functionals. In this work we introduce a framework for $2\nu\beta\beta$ decays based on a relativistic nuclear energy density functional [88]. In the relativistic nuclear energy density functional (REDF) framework, the nuclear ground-state density and energy are determined by the self-consistent solution of relativistic single-nucleon Kohn-Sham equations [89,90]. In the present study these equations are implemented through an interaction Lagrangian density formulated in terms of the relevant degrees of freedom. Since the REDF has already been extensively used in many previous studies, here we give only a brief overview of the relevant foundations of this framework. Two different families of relativistic density-dependent interactions are used in this work, (i) finite range meson-exchange and (ii) point-coupling interactions. In the former case, pointlike nucleons interact through the exchange of light mesons, namely, ω, ρ, and σ mesons, in addition to an electromagnetic interaction mediated by photons. The model is explained in detail in Refs. [88,91–94]. Meson-nucleon couplings are established as functions of the vector density, motivated by the relativistic Brueckner-Hartree-Fock calculations, but introduced through a phenomenological ansatz with parameters adjusted to the experimental data in finite nuclei [88]. In this work, the DD-ME2 parametrization of the density-dependent meson-exchange interaction is used [91], being one of the most successful parametrizations currently used in the description of a variety of nuclear properties and astrophysically relevant processes [63,95,96].

In the case of point-coupling interactions, the effective Lagrangian contains four fermion contact interaction terms

including the isoscalar-scalar, isoscalar-vector, isovector-vector, and isospace-space channels, coupling of protons to the electromagnetic field, and the derivative term accounting for the leading effects of finite-range interactions necessary for a quantitative description of nuclear density distribution and radii (for more details see Refs. [88,97]). In our study of $2\nu\beta\beta$ decays, two parametrizations of the density-dependent point-coupling interactions are used, DD-PC1 [97] and the more recently established DD-PCX [98]. While the DD-PC1 interaction is adjusted to nuclear binding energies, the DD-PCX interaction is specifically adjusted both to the nuclear ground state and excitation properties, in order to constrain not only the nuclear properties but also the symmetry energy close to the saturation density, and the incompressibility of nuclear matter by using genuine observables on finite nuclei in the χ^2 minimization [98].

For the description of ground-state properties of open-shell nuclei a unified and self-consistent treatment of mean-field and pairing correlations is needed. In this work we employ the relativistic Hartree-BCS (RH-BCS) theory [58,82] which represents a relativistic extension of the nonrelativistic Hartree-Fock-BCS framework [99,100]. Spherical symmetry is assumed. The pairing correlations in the ground state are described using a separable pairing force, which also includes two parameters for the pairing strength (G_p and G_n) [101]. While in the RH-BCS model with DD-ME2 and DD-PC1 interactions the pairing parametrization from Ref. [101] is used, the DD-PCX interaction is supplemented with its own parametrization for the separable pairing force as given in Ref. [98]. Within the RH-BCS model, the isoscalar pairing is not included; i.e., no proton-neutron mixing is considered.

B. Proton-neutron relativistic QRPA

Charge-exchange transitions between the states in nuclides involved in $2\nu\beta\beta$ decay are described in the framework of the proton-neutron relativistic quasiparticle random phase approximation (REDF-QRPA). An introduction to the charge-exchange QRPA (or proton-neutron QRPA, pn-QRPA) calculations can be found in Refs. [102,103], while in the relativistic framework it has been introduced in Refs. [67,104]. The residual REDF-QRPA interaction is derived from the relativistic formulation of the effective Lagrangian density, and throughout the calculation of the QRPA matrix elements, the Dirac wave functions from the RH-BCS model, including both large and small components, are systematically included. In addition, the transition operators are also extended for their implementation in the relativistic framework. More details on the relativistic QRPA are given in Refs. [67,95,104–106]. Here we give only a brief overview of the REDF-QRPA adopted for the purpose of the study of $2\nu\beta\beta$ decay. The states in the intermediate $(Z+1, N-1)$ nucleus are REDF-QRPA phonons:

$$|m\rangle = \sum_{pn} \left[X_{pn} a_p^\dagger a_n^\dagger - Y_{pn} a_n a_p\right] |\text{QRPA}\rangle\,, \tag{10}$$

where the creation operators $a^\dagger_{p(n)}$ create a proton (neutron) state in an orbital labeled p (n), and quantities X and Y are, as noted earlier, the REDF-QRPA amplitudes. $|\text{QRPA}\rangle$ denotes the QRPA vacuum, which we take to be the ground state (see Sec. III A). By linearizing the time-dependent RH-BCS equations in charge-exchange external field, the charge-exchange QRPA equations are obtained [79]:

$$\begin{pmatrix} A & B \\ -B^* & -A^* \end{pmatrix} \begin{pmatrix} X(J) \\ Y(J) \end{pmatrix} = \omega_k \begin{pmatrix} X(J) \\ Y(J) \end{pmatrix}, \tag{11}$$

where the REDF-QRPA matrices A and B are defined as

$$\begin{aligned} A_{pnp'n'}(J) = {} & (E_p + E_n)\delta_{pp'}\delta_{nn'} + (u_p u_{p'} u_n u_{n'} \\ & + v_p v_{p'} v_n v_{n'}) \langle pnJ| V |p'n'J\rangle + (u_p v_{p'} u_n v_{n'} \\ & + v_p u_{p'} v_n u_{n'}) \langle pn^{-1}J| V_{res} |p'n'^{-1}J\rangle\,, \end{aligned} \tag{12}$$

and

$$\begin{aligned} B_{pnp'n'}(J) = {} & (u_p u_{p'} v_n v_{n'} + v_p v_{p'} u_n u_{n'}) \langle pnJ| V |p'n'J\rangle \\ & + (u_p v_{p'} v_n u_{n'} + v_p u_{p'} u_n v_{n'}) \langle pn^{-1}J| \\ & \times V_{res} |p'n'^{-1}J\rangle\,, \end{aligned} \tag{13}$$

where V_{res} is the residual interaction derived from the relativistic nuclear energy density functional, while V includes the pairing interaction in the QRPA [67,68], $u_{p(n)}$, $v_{p(n)}$ being proton (neutron) RH-BCS amplitudes. The residual interaction V_{res} is derived from the same effective meson-exchange or point-coupling interaction as used in the ground-state calculations (see Sec. III A). In addition, the pseudovector interaction channel is also included, and its strength parameter was previously constrained to the experimental data on Gamow-Teller resonance in ^{208}Pb [67,68,95].

The REDF-QRPA equations include both the isovector ($T=1$) and isoscalar ($T=0$) pairing channels, described by the separable interaction [68,69,101]

$$V^{pn}(r_1, r_2) = -fG\delta(\boldsymbol{R} - \boldsymbol{R}')P(r)P(r')(1 - P^r P^\sigma P^\tau), \tag{14}$$

where the projectors $P^{r,\sigma,\tau}$ are defined as usual, G is the overall interaction strength, R and r are center of mass and relative coordinates, respectively, and $P(r)$ is defined as

$$P(r) = \frac{1}{(4\pi a^2)^{3/2} e^{-\frac{r^2}{2a^2}}}. \tag{15}$$

The overall strength in the pairing channel is multiplied by a dimensionless factor f defined as

$$f = \begin{cases} 1, & T=1, S=0 \\ V_{0pp}, & T=0, S=1 \\ 0, & \text{otherwise}, \end{cases} \tag{16}$$

where V_{0pp} represents the isoscalar pairing strength. For the $T=1$ channel, the same separable pairing interaction is used as in the RH-BCS model (see Sec. III A). The strength parameters $G_{p(n)}$ for protons (neutrons) and the width a are defined in Ref. [107], but other parametrizations also exist, e.g., the one constrained with the DD-PCX interaction [98]. For the $T=0$ channel, the pairing strength parameter V_{0pp} has to be constrained at the level of REDF-QRPA, e.g., by using experimental data on Gamow-Teller transitions or β decays. In our treatment of $2\nu\beta\beta$ decay, this allows us to explore the dependence of the NME on the pairing strength parameter

TABLE I. The fit parameters for the $T = 0$ pairing strength functional form in Eq. (19) obtained from the optimization on β-decay half-lives for the models with DD-PCX, DD-PC1, and DD-ME2 interactions.

	DD-ME2	DD-PC1	DD-PCX
V_1	0.574 ± 0.338	0.522 ± 0.407	0.592 ± 0.366
V_2	2.301 ± 1.422	3.092 ± 1.768	2.321 ± 1.559

V_{0pp}, showing the variation in the possible values for the matrix elements. However, to provide predictions on $2\nu\beta\beta$ decay matrix elements, in this work V_{0pp} is also constrained by the experimental data on single-β-decay half-lives (Sec. III C).

The transition matrix elements necessary for $2\nu\beta\beta$ NMEs in Eq. (3) are given by the following expressions [44]:

$$\langle i|\sum_a \sigma_a \tau_a^- |m\rangle = \sum_{pn} \langle p||\boldsymbol{\sigma}||n\rangle \left[u_p v_n X_{pn}^m + v_p u_n Y_{pn}^m\right] \quad (17)$$

$$\langle m|\sum_a \sigma_a \tau_a^+ |f\rangle = \sum_{pn} \langle p||\boldsymbol{\sigma}||n\rangle \left[v_p u_n X_{pn}^m + u_p v_n Y_{pn}^m\right]. \quad (18)$$

Here, the terms next to the X and Y amplitudes represent particle-type and hole-type one-quasiparticle transitions, respectively [79].

C. Determination of the isoscalar pairing strength

In order to constrain the isoscalar ($T = 0$) pairing strength V_{0pp} we use a similar approach as suggested in Refs. [81,82,108], namely, V_{0pp} is determined from the global fit of β-decay half-lives to experimental data. We have used even-even nuclei in the range $8 \leqslant Z \leqslant 82$ for which experimental data on β-decay half-lives is available, where V_{0pp} has the effect in the relative change of half-lives $T_{1/2}$ by more than 20%, and whose half-lives are $<10^3$ s. In this way we have additionally optimized the fitting procedure, because too-long half-lives may be challenging for quantitative description within the QRPA method [81]. Since the isoscalar pairing strength V_{0pp} shows isotopic dependence [81], in the fitting procedure we use a functional form,

$$V_{0pp} = V_1 + V_2\left(\frac{N-Z}{A}\right), \quad (19)$$

that appears to provide a comparable quality of the fit to β-decay half-lives to other previously used functional forms [81]. The β-decay half-lives are calculated using the REDF-QRPA as described in Ref. [82], including both allowed and first-forbidden transitions. We used the same quenched value of axial coupling, $g_A = 1.0$, as in this work. The fitting procedure determines V_{0pp} which reproduces the experimental β-decay half-lives. Here we note that only those V_{0pp} which yield real solutions of the QRPA equation should be included in the fit to the proposed ansatz. Using models with DD-ME2, DD-PC1, and DD-PCX interactions, the obtained average values of the fitted parameters V_1 and V_2 as well as 1σ uncertainties are given in Table I. This results in a rather narrow range of values for the isoscalar pairing strength V_{0pp} for the set of nuclei considered in $2\nu\beta\beta$ decay study in this work. The respective values for V_{0pp} with the uncertainties are given in Table II. In the following section we refer to *optimal* V_{0pp} when using the values from Table II. We note that most of the V_{0pp} values are close to 1.0, meaning the strengths of the isoscalar and isovector pairing are very similar, which in turn points to a "soft" breaking of spin-isospin SU(4) symmetry in present calculations.

TABLE II. Optimal values of the $T = 0$ pairing strength parameter V_{0pp} constrained from the β-decay half-lives.

	V_{0pp}		
	DD-ME2	DD-PC1	DD-PCX
^{48}Ca	0.98 ± 0.12	1.04 ± 0.12	0.96 ± 0.11
^{76}Ge	0.96 ± 0.13	1.01 ± 0.14	0.94 ± 0.12
^{82}Se	0.99 ± 0.11	1.05 ± 0.12	0.97 ± 0.10
^{96}Zr	0.98 ± 0.12	1.04 ± 0.12	0.96 ± 0.11
^{100}Mo	0.96 ± 0.13	1.02 ± 0.13	0.94 ± 0.12
^{116}Cd	0.99 ± 0.11	1.06 ± 0.11	0.97 ± 0.10
^{124}Xe	0.89 ± 0.17	0.92 ± 0.18	0.87 ± 0.16
^{128}Te	1.07 ± 0.07	1.16 ± 0.07	1.05 ± 0.07
^{130}Te	1.03 ± 0.09	1.10 ± 0.09	1.01 ± 0.08
^{136}Xe	1.06 ± 0.08	1.14 ± 0.08	1.03 ± 0.07
^{150}Nd	1.06 ± 0.08	1.14 ± 0.08	1.03 ± 0.07

IV. RESULTS AND DISCUSSION

By employing the framework of a relativistic theory for nuclear properties and transitions as outlined in the previous sections, we performed calculations of the $2\nu\beta\beta$ decay matrix elements. In the first step, the RH-BCS model [88] is used to describe the ground-state properties of the initial and final nuclei involved in the decay. The RH-BCS model is formulated in the harmonic oscillator basis and we restrict calculations to 20 oscillator shells both for protons and neutrons. The single-particle wave functions and the corresponding occupation probabilities in the RH-BCS quasiparticle basis are used in the REDF-QRPA to describe GT transitions involved in the $2\nu\beta\beta$ decay. The REDF-QRPA calculations are performed in two steps, for β^- (β^+) matrix elements for decays from the initial (final) nucleus to the intermediate nucleus, which are then used to calculate the $2\nu\beta\beta$ decay NME. All the other quantities that appear in the calculations, including the energies of the intermediate states and the Q values, are also taken self-consistently from the RH-BCS and REDF-QRPA calculations. To assess the information on the model dependence of the $2\nu\beta\beta$ decay NME, three relativistic energy density functionals are used in the study, including the density-dependent meson-exchange interaction with the DD-ME2 parametrization [91], and density-dependent point-coupling interactions DD-PC1 [97], and the more recently established DD-PCX [98]. One of the open questions in the description of double-β decays is the problem of quenching of the axial-vector coupling constant g_A, which has attracted attention in many recent studies (e.g., see Refs. [2,7]). As already mentioned above, $g_A = 1.0$ is systematically used in the present study.

Throughout this section we provide the absolute values of the $2\nu\beta\beta$ decay matrix elements, since only the squares of

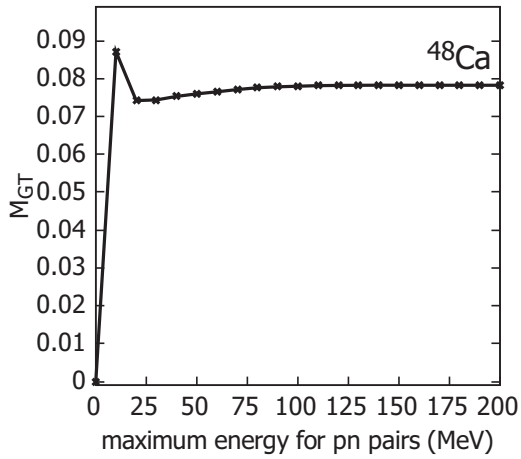

FIG. 1. The NMEs for $2\nu\beta\beta$ decay based on Gamow-Teller transitions, shown as a function of the maximal two-quasiparticle energy. The DD-ME2 interaction is used in calculations. Matrix elements are dimensionless.

their absolute values have physical significance. The REDF-QRPA calculations are first performed to set the cutoff energy for the quasiparticle pairs that compose the configuration space. To all relevant configurations, a convergence test is performed in order to restrict the maximal two-quasiparticle energy with the condition that the value of the NME converges with increasing energy. We illustrate the convergence of the NME values in Fig. 1 for the case of ^{48}Ca, where the matrix elements are shown as a function of the maximal proton-neutron two-quasiparticle energy $E_{2qp}^{\max}$. The DD-ME2 effective interaction is used for this demonstration. The GT transitions are considered. One can observe that the NMEs converge with high accuracy at two-quasiparticle energy $E_{2qp}^{\max} \approx 100$ MeV.

Insight into the contributions of various states to the final NMEs can be obtained from the running sum, which includes the sum of all contributions to the matrix element up to a specific maximal excitation energy in the intermediate nucleus [109] which we denote as E_{exc} in the following discussion.

Figures 2 and 3 show the respective running sums for the Gamow-Teller double-β decay transitions for ^{48}Ca and ^{76}Ge, displayed as functions of E_{exc}. The sums are taken at two values of the $T = 0$ pairing strength parameter, $V_{0pp} = 0$, representing a situation where isoscalar pairing vanishes, and the optimal values $V_{0pp} = 0.98$ and 0.96 for ^{48}Ca and ^{76}Ge, respectively. One can observe that for ^{48}Ca the hypothesis of single-state dominance [110] holds in the REDF-QRPA calculations; i.e., most of the contribution to the NMEs mainly comes from a single low-lying state in the intermediate nucleus. For ^{76}Ge, many states contribute to M_{GT} up to 20 MeV, and in some cases destructive interference in their contributions to the NMEs is obtained. The same dependence is shown in Fig. 4 for other nuclei considered in this work, from ^{82}Se to ^{150}Nd, using optimal values of V_{0pp}. We see that generally the single-state dominance (SSD) hypothesis is approximatively fulfilled, although in some cases more complicated structure is obtained due to contributions from

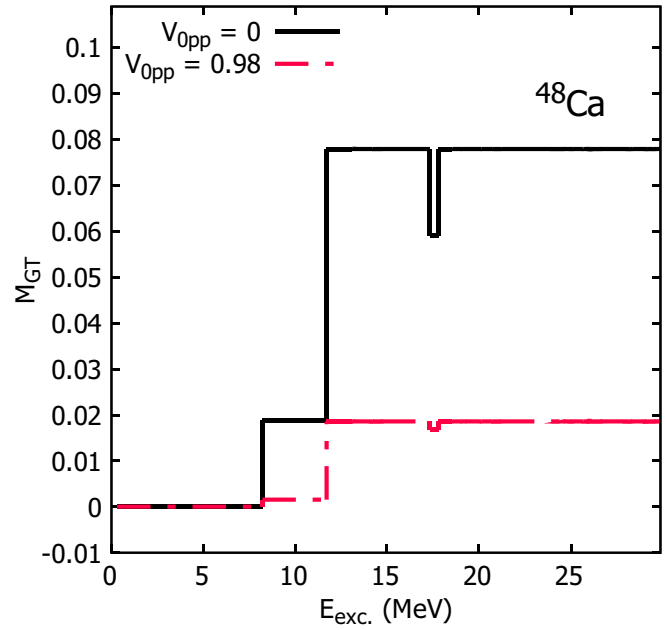

FIG. 2. The running sum of the GT NMEs for the $2\nu\beta\beta$ decay of ^{48}Ca for the DD-ME2 interaction, shown as a function of maximal excitation energy E_{exc} in the intermediate nucleus. The cases with and without $T = 0$ pairing are shown separately.

several states. Particularly noticeable are significant cancellations when the nuclear matrix element is significantly lowered from the value at zero isoscalar pairing due to a high value of V_{0pp}. It is interesting to note that presented results for some nuclei are in reasonable agreement with recent experimental results, which show that the SSD hypothesis holds for ^{100}Mo [111], while for ^{82}Se we obtain a more complex structure than the SSD measured in Ref. [112]. Our results

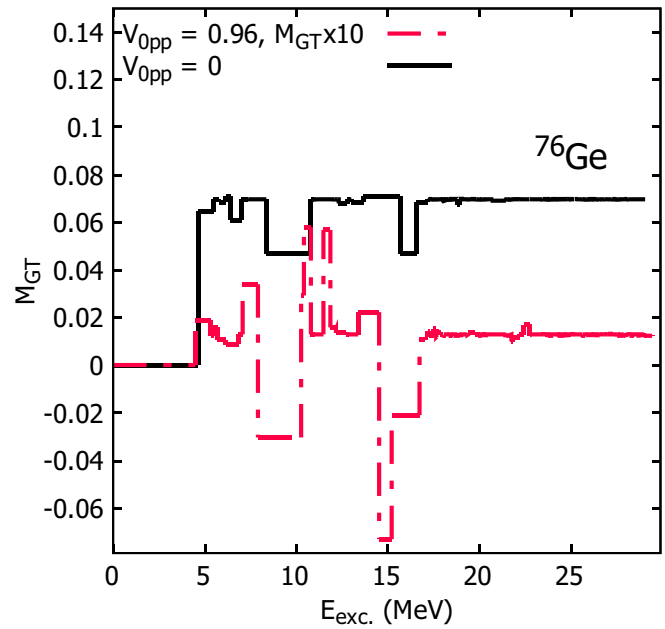

FIG. 3. The same as in Fig. 2, but for ^{76}Ge.

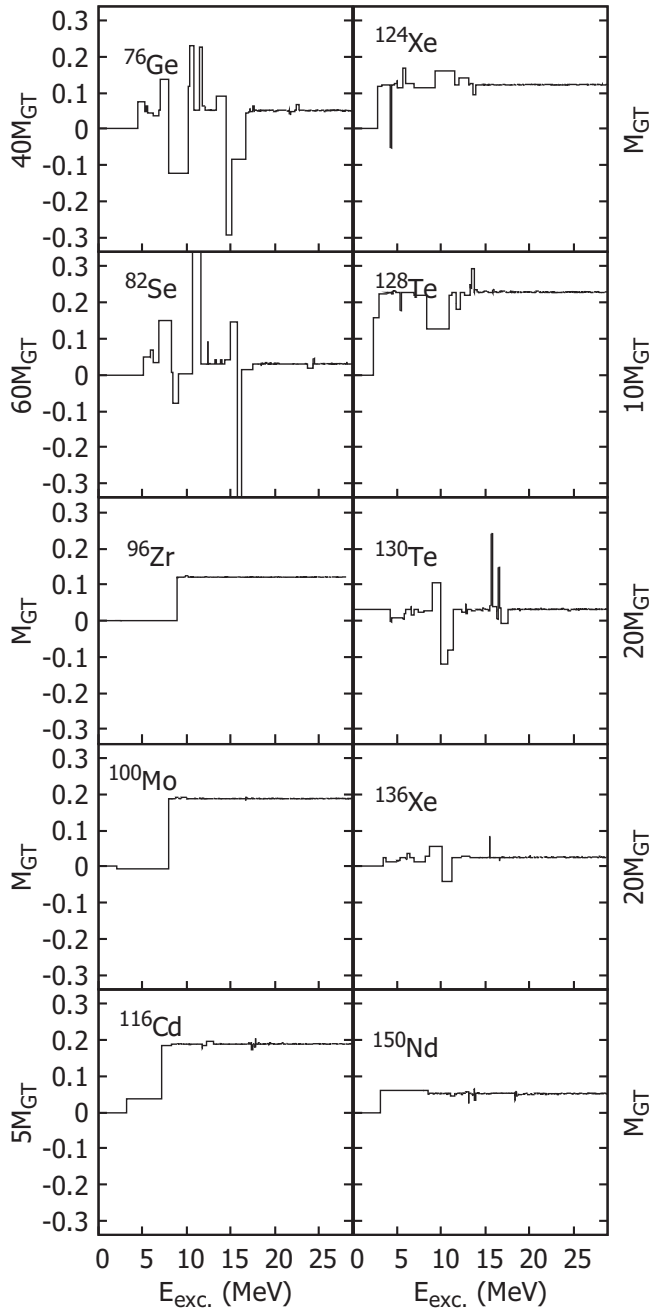

FIG. 4. Running sums for the GT NMEs for DD-ME2 interaction and optimal values of V_{0pp} from Table II, for the $2\nu\beta\beta$ decays of ^{82}Se–^{150}Nd, shown as a function of maximal excitation energy $E_{\rm exc}$ in the intermediate nucleus.

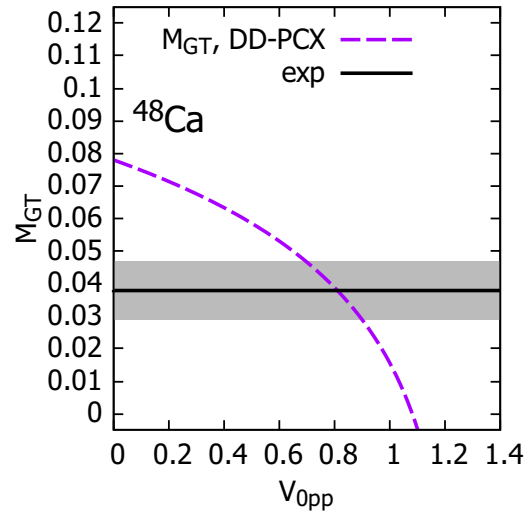

FIG. 5. The dependence of the GT NMEs for $2\nu\beta\beta$ decay on the isoscalar pairing strength V_{0pp} for ^{48}Ca, using DD-ME2 interaction, in comparison to the result obtained from the experimental data on $2\nu\beta\beta$ decay [80].

for the running sum in ^{136}Xe are at variance with the experimental results in Ref. [113]. In the same study, it was shown that the running sum is strongly model dependent, resulting in considerable differences between the reported QRPA and shell model calculations [113]. Our results also differ from other calculations of running sums, including also contributions with a negative sign. They appear and become more prominent with increasing V_{0pp}, and cancel out to a large extent an initially large NME, and the fact that we show the running sums at higher optimal V_{0pp} value explains in part their appearance.

Before systematic implementation of the optimal values of V_{0pp} from Table II in model calculations, it is interesting to explore the general dependence and sensitivity of the $2\nu\beta\beta$ decay NMEs on V_{0pp}. In Fig. 5 the dependence of the absolute values of nuclear matrix elements is shown for ^{48}Ca as a function of V_{0pp}. The black line in the figure represents the value of the nuclear matrix element deduced from the experimental data on $2\nu\beta\beta$ half-lives [80,114]. The grey band around this line denotes an uncertainty at the level of 3σ. As one can see in Fig. 5, the NME systematically decreases with V_{0pp}, and an overlap between the calculated curve and the experimental limit for the NMEs is obtained. Here, the overlap prescription given in Eq. (7) is used. We have verified that the result using the overlap prescription in Eq. (7) appears almost identical to the one given in Eq. (8). Figure 6 shows the difference between the NMEs for ^{48}Ca obtained using these two methods for calculating the overlap, given as a function of V_{0pp}. One can observe that not only the difference is small, but it also reduces as one approaches the V_{0pp} value deduced from the experiment as the optimal one, as shown in Fig. 5. Therefore, in the following investigation we consider only the results based on the overlap prescription given in Eq. (7).

A quantity related to the NMEs that has received recent theoretical and experimental interest [115,116] is the function $C(r)$, representing the contribution to the NME at a given internucleon distance $r_{12} \equiv r$. It is related to the NME, denoted here as $\mathcal{M}$, as

$$\int_0^\infty dr C(r) = \mathcal{M}. \tag{20}$$

Figure 7 shows the $C(r)$ function for $2\nu\beta\beta$ decay of ^{48}Ca, obtained using the DD-ME2 interaction for the range of values of $T = 0$ pairing strength parameters V_{0pp}. The quantity is

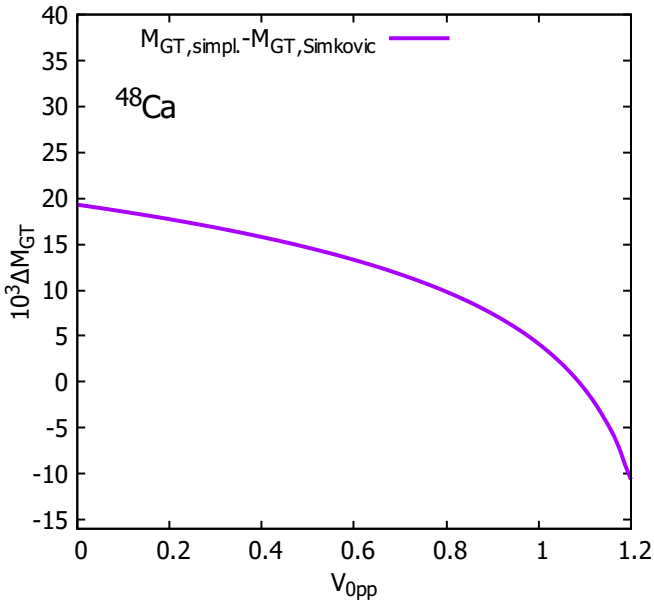

FIG. 6. The difference between the NMEs calculated using two prescriptions for the GT $2\nu\beta\beta$ decay matrix element, shown as a function of the isoscalar pairing strength V_{0pp} (see text for details). "$M_{GT,simpl.}$" refers to the usual prescription for the overlap factor in Eq. (7), while "$M_{GT,Simkovic}$" refers to the prescription in Eq. (8).

evaluated in the closure approximation and is directly connected to the dimensionless NME. It needs to be noted that, due to the computational resources necessary for the evaluation of the $C(r)$ function, the results we report have been calculated at a lower energy cutoff than the results for the NMEs in the present work, specifically at 50 MeV. Comparing the $C(r)$ function to those calculated in Ref. [116] we conclude that qualitatively the same shape is obtained, with a sharp peak around 1 fm, converging to zero with an increase of r. This result is consistent with the findings that this shape is universal for $2\nu\beta\beta$ decay [117], although our

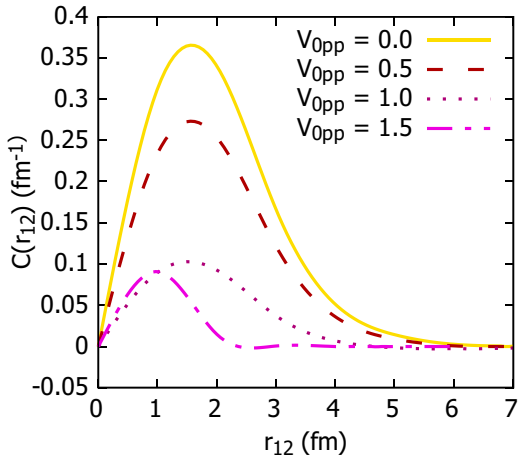

FIG. 7. The function $C(r_{12})$, showing the contributions to the NME at nucleon separations r_{12}, for the Gamow-Teller $2\nu\beta\beta$ decay of ^{48}Ca, for V_{0pp} from 0.0 to 1.5.

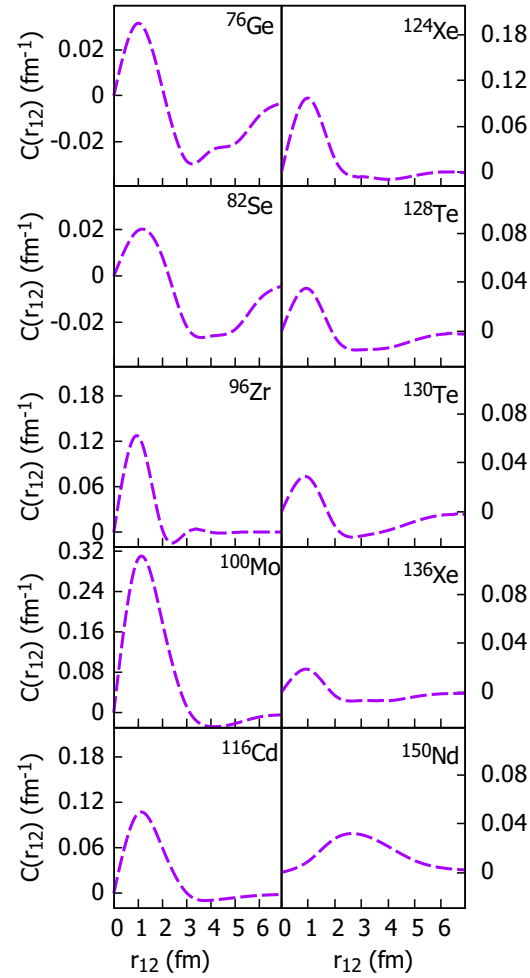

FIG. 8. The function $C(r_{12})$, showing the contributions to the NME at nucleon separations r_{12}, for the Gamow-Teller $2\nu\beta\beta$ decay of ^{76}Ge–^{150}Nd, evaluated at optimal values of V_{0pp}.

model does not contain $S = 0$ pairing in the $T = 0$ channel, as well as $T = 0$ channel in the ground state. The behavior obtained with increasing $T = 0$ pairing strength V_{0pp} in the residual QRPA interaction is also consistent with previous studies [116]; i.e., the $C(r)$ function reaches its highest values when pairing is not taken into account and with the increase of the pairing strength the central peak becomes reduced. We would note that the contribution of high internucleon distances in many nuclei is negative and serves to lower the NME; these negative contributions, once again, become more noticeable with increasing V_{0pp}. The same function, for other nuclides considered in this work up to ^{150}Nd, evaluated using the DD-ME2 interaction and optimal values of V_{0pp}, is shown in Fig. 8. Similar general behavior of the $C(r_{12})$ function is obtained for all nuclei, that peaks strongly at low r_{12} values. Where the NMEs are close to zero, we can note significant cancellations as one integrates the $C(r)$ function over the internucleon distance r. ^{150}Nd is an exception to the general rule that the first and most prominent peak of the function is near 1 fm, with a dominant peak at significantly higher radii. This suggests that the results for ^{150}Nd should be taken with

less certainty than those for other nuclides. However, we need to point out that in certain cases our $C(r)$ functions also show contributions at higher internucleon distances than is found in previous QRPA calculations. We note that the contribution of high internucleon distances in many nuclei is negative and serves to lower the NME; these negative contributions, once again, become more noticeable with increasing V_{0pp}.

The GT transitions relevant for the $2\nu\beta\beta$ decay of ^{48}Ca were studied experimentally in Ref. [118]. The GT$^-$ and GT$^+$ strength distributions in ^{48}Sc were measured by the ^{48}Ca(p, n) and ^{48}Ti(n, p) reactions, respectively. The integrated GT strengths up to an excitation energy of 30 MeV in ^{48}Sc obtained from (p, n) and (n, p) spectra amount to $B(\mathrm{GT}^-) = 15.3 \pm 2.2$ and $B(\mathrm{GT}^+) = 2.8 \pm 0.3$. The REDF-QRPA calculations with DD-ME2 interaction for the corresponding transitions result in $B(\mathrm{GT}^-) = 23.47$ and $B(\mathrm{GT}^+) = 3.48$; thus the experiment provides 65% of GT$^-$ strength and 80% of the GT$^+$ strength obtained in model calculations. Clearly, further experimental studies of GT transitions are needed to provide more transition strength that is relevant for double-β decays. The missing strength in measured GT spectra has been confirmed in recent REDF-QRPA calculations for other nuclei in Ref. [68], and studies going beyond the RPA level including couplings between single-nucleon and collective nuclear vibrations could not resolve the discrepancy between the theoretical and experimental GT strengths [119].

In the following, the NMEs are investigated for the set of nuclides usually considered in $2\nu\beta\beta$ decay studies because there are experimental data available: ^{48}Ca, ^{76}Ge, ^{82}Se, ^{96}Zr, ^{100}Mo, ^{116}Cd, ^{128}Te, ^{130}Te, ^{136}Xe, ^{150}Nd, and most recently ^{124}Xe. Figure 9 shows the NMEs for the set of 11 nuclides listed above, given as a function of the isoscalar pairing strength V_{0pp}. The results extracted from the experimental data on $2\nu\beta\beta$ decay half-lives are shown for comparison [114]. We conclude that the dependence of the nuclear matrix elements on V_{0pp} is qualitatively similar for all nuclei considered, with the values of the GT-based NMEs decreasing and their slopes increasing, with increasing absolute values of V_{0pp}. However, there is a significant variation in the values of V_{0pp} needed to reproduce the NMEs based on experimental data. A similar issue has been observed in β-decay studies [81], indicating that some mass dependence is necessary for the optimization of the isoscalar pairing channel in the residual interaction of the REDF-QRPA, as we have also discussed in Sec. III C.

To assess the information about the model dependence of the $2\nu\beta\beta$ decay matrix elements, we conducted a detailed comparison of our results with a selection of previous studies. A direct comparison of the results of the present study with those from previous calculations can be difficult both due to different theoretical frameworks and parametrizations used.

In Ref. [1], the pn-QRPA matrix elements are given for several $A > 100$ nuclides, using a value of the $T = 0$ pairing strength $g_{pp} = 0.7$. A comparison with the REDF-QRPA results with $V_{0pp} = 0$ is given in Table III. We see that the upper limit of NMEs in the present study remains lower than those reported by other pn-QRPA calculations.

Further comparison can be made with the recent pn-QRPA results of Šimkovic *et al.* [84], which is done in Table IV. We note that the values from Ref. [84], except for ^{48}Ca and ^{82}Se, are in excellent agreement with our results, even though the latter were obtained with vanishing isoscalar pairing. We also note that the NMEs given in Ref. [84] are effective matrix elements obtained with a quenched value of $g_A = 0.904$. The renormalization factor was split according to isospin channel into $g_{pp}^{T=1}$ and $g_{pp}^{T=0}$; the values of both parameters for each respective nucleus are given in Table IV.

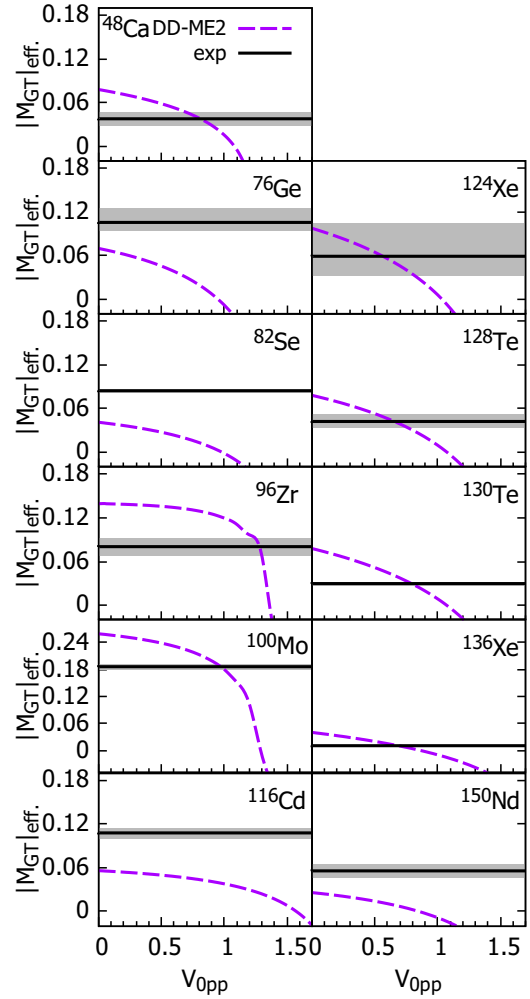

FIG. 9. The dependence of the NMEs for $2\nu\beta\beta$ decay on the isoscalar pairing strength V_{0pp} for $48 < A < 150$ nuclei that decay through the $2\nu\beta\beta$ channel, in comparison to the result obtained from the experimental data [80].

TABLE III. The NMEs for $2\nu\beta\beta$ decay based on the REDF-QRPA (DD-ME2 interaction, $V_{0pp} = 0$) and the NMEs based on the pn-QRPA from Ref. [1].

	REDF-QRPA (DD-ME2)	pn-QRPA [1]
^{100}Mo	0.259	0.6560
^{116}Cd	0.056	0.2169
^{128}Te	0.078	0.1041
^{130}Te	0.079	0.1066

TABLE IV. The NMEs for $2\nu\beta\beta$ decay based on the REDF-QRPA (DD-ME2 interaction, $V_{0pp} = 0$) and the NMEs based on the pn-QRPA from Ref. [84] with the pairing strength parameters $g_{pp}^{T=1}$ and $g_{pp}^{T=0}$ given in the last two columns.

	REDF-QRPA (DD-ME2)	pn-QRPA [84]	$g_{pp}^{T=1}$ [84]	$g_{pp}^{T=0}$ [84]
^{48}Ca	0.078	0.019	1.028	0.745
^{76}Ge	0.070	0.077	1.021	0.733
^{82}Se	0.041	0.071	1.016	0.737
^{96}Zr	0.140	0.162	0.961	0.739
^{100}Mo	0.259	0.306	0.985	0.799
^{116}Cd	0.056	0.059	0.892	0.877
^{128}Te	0.078	0.076	0.965	0.741
^{130}Te	0.079	0.065	0.963	0.737

Next, in Table V we compare the NMEs using the REDF-QRPA (DD-ME2 interaction, $V_{0pp} = 0$ MeV) with those of recent interacting boson model (IBM) calculations [36,120]. The IBM results have been calculated within a closure approximation, and to allow for a direct comparison, the values we report for the NMEs were obtained in the closure approximation as well. To obtain NMEs comparable to our own from the NMEs quoted by Barea and Iachello, which do not include the energy denominator, we divide the NMEs with an average energy denominator as tabulated in Ref. [121]. The resulting NMEs based on the IBM are generally larger, but comparable to the REDF-QRPA results. The inclusion of isoscalar pairing in the REDF-QRPA residual interaction would further increase this difference. This result suggests an advantage of our calculations over the IBM, as the experimental values are even lower for most nuclei considered and, for most nuclei, are within the reach of the REDF-QRPA with a suitable choice of V_{0pp}.

Further comparison is made with the interacting shell model (ISM) [112], as shown in Table VI. Since the ISM contains isoscalar pairing as a significant effect, we compare the shell model results to those of the REDF-QRPA calculated at the optimal pairing strength V_{0pp} as given in Table II. The REDF-QRPA results are considerably smaller than those of the ISM.

TABLE V. The NMEs for $2\nu\beta\beta$ decay based on the REDF-QRPA (DD-ME2 interaction, $V_{0pp} = 0$), calculated in the closure approximation, and the results of the interacting boson model (IBM) [120].

	REDF-QRPA (DD-ME2)	IBM [120]
^{48}Ca	0.121	0.213
^{76}Ge	0.110	0.471
^{82}Se	0.071	0.356
^{96}Zr	0.125	0.208
^{100}Mo	0.210	0.272
^{116}Cd	0.056	0.197
^{128}Te	0.079	0.308

TABLE VI. The NMEs for $2\nu\beta\beta$ decay based on the REDF-QRPA (DD-ME2 interaction, optimal V_{0pp}), and the results of the interacting shell model (ISM) (Ref. [112] unless otherwise noted).

	REDF-QRPA (DD-ME2)	ISM [112]
^{48}Ca	0.019	0.026
^{76}Ge	0.001	0.104
^{82}Se	0.001	0.109
^{124}Xe [122]	0.023	0.028–0.072
^{128}Te [123]	0.006	0.030
^{130}Te	0.002	0.061
^{136}Xe [123]	0.001	0.013

More recent pn-QRPA results can be found in Ref. [124], but only for some of the nuclei considered in this work. The parameters for the calculation are determined using two procedures, fitting of the ft values (product of the Fermi integral and β-decay half-life) [125] to an isobaric triplet and multiplet. The comparison to the NMEs based on the REDF-QRPA with optimal V_{0pp} is given in Table VII, showing reasonable agreement for ^{100}Mo, while for ^{116}Cd and ^{128}Te the REDF-QRPA provides smaller NMEs.

Finally, we compare our calculations with the results of a recent effective theory (ET) treatment of double-β decay [126]. Effective theories concern the behavior of nuclei at suitably low energies, which is described in terms of low-energy collective degrees of freedom, with any influence from high-energy physics being encoded into the low-energy constants which are fitted to available experimental data. The effective theory described in Ref. [126] takes as its degrees of freedom nucleons and quadrupole phonon excitations of an even-even spherical core the nucleons are coupled to. The comparison of REDF-QRPA results using DD-ME2 interaction and optimal V_{0pp}, with those of the ET, is given in Table VIII. With the exception of ^{100}Mo, our results are systemically smaller, although they are comparable to the effective theory result in the case of ^{116}Cd.

One of the open questions in the description of double-β decays is optimization of the strength parameter of the isoscalar pairing in the residual QRPA interaction. Since this interaction channel is difficult to constrain, and in most of the models cannot be determined based on the ground-state properties, it is necessary to explore its role in the NMEs for double-β decays. In the present study, the experimental data on β-decay half-lives are used to constrain the value

TABLE VII. The NMEs for $2\nu\beta\beta$ decay based on the REDF-QRPA (DD-ME2 interaction, optimal V_{0pp}), and recent results of the proton-neutron QRPA (pn-QRPA) (Ref. [124]).

	REDF-QRPA (DD-ME2)	pn-QRPA [124] triplet	pn-QRPA [124] multiplet
^{100}Mo	0.189	0.153	0.131
^{116}Cd	0.038	0.153	0.160
^{128}Te	0.006	0.069	0.095

TABLE VIII. The NMEs for $2\nu\beta\beta$ decay based on the REDF-QRPA (DD-ME2 interaction, optimal V_{0pp}), and the results of the effective theory outlined in Ref. [126].

	REDF-QRPA (DD-ME2)	ET [126]
^{76}Ge	0.001	0.054
^{82}Se	0.001	0.097
^{100}Mo	0.189	0.111
^{116}Cd	0.038	0.085
^{128}Te	0.006	0.031
^{130}Te	0.002	0.021

of the isoscalar pairing strength parameter V_{0pp} (Sec. III C), and in this way the REDF-QRPA can provide predictions for $2\nu\beta\beta$ decay properties. Figure 10 shows the NME for $2\nu\beta\beta$ decay nuclides from ^{48}Ca up to ^{150}Nd, obtained using the REDF-QRPA with the DD-ME2 interaction, for the range of values for $V_{0pp} = 0$–1. The experimental data adopted from Ref. [80] are also shown for comparison. One can observe a systematic decrease of the NMEs with increasing the value of V_{0pp}. For several nuclei, the experimentally determined NMEs (with their error bars) are within the range of calculated NMEs when considering the full range of V_{0pp} values from 0 to 1. The exceptions are ^{76}Ge, ^{82}Se, ^{96}Se, ^{116}Cd, and ^{150}Nd where the calculated NMEs are smaller (also the experimental errors are rather small), and ^{96}Zr where the calculated NMEs are larger. In the case of ^{116}Cd and ^{96}Zr the differences between

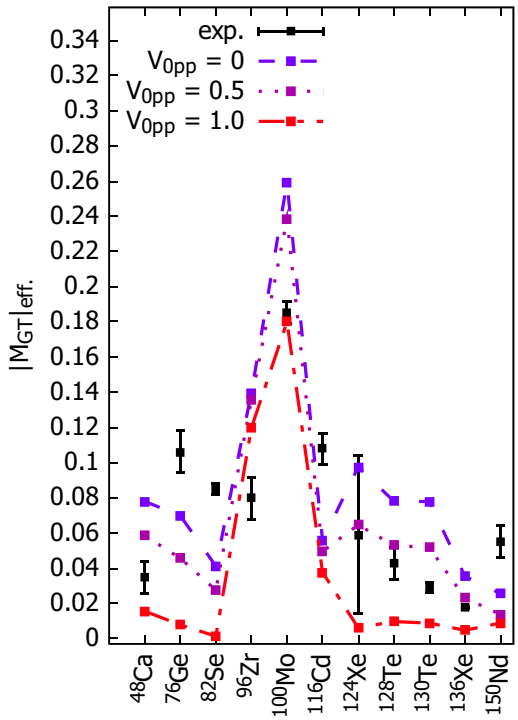

FIG. 10. The dependence of the NME for $2\nu\beta\beta$ decay on the isoscalar pairing strength V_{0pp} for $A = 48$–150 nuclides.

TABLE IX. The NMEs for $2\nu\beta\beta$ decay obtained with the DD-ME2 interaction and optimal values of V_{0pp} given in Table II, and NMEs obtained from the experimental data.

	REDF-QRPA (DD-ME2)	Expt. [127]
^{48}Ca	$0.019^{+0.014}_{-0.019}$	0.035 ± 0.003
^{76}Ge	$0.001^{+0.024}_{-0.001}$	0.106 ± 0.004
^{82}Se	$0.001^{+0.011}_{-0.001}$	0.085 ± 0.001
^{96}Zr	$0.121^{+0.006}_{-0.010}$	0.080 ± 0.004
^{100}Mo	$0.189^{+0.020}_{-0.033}$	0.185 ± 0.002
^{116}Cd	$0.038^{+0.004}_{-0.004}$	0.108 ± 0.003
^{124}Xe	$0.023^{+0.021}_{-0.023}$	0.059 ± 0.015
^{128}Te	$0.006^{+0.011}_{-0.006}$	0.043 ± 0.003
^{130}Te	$0.002^{+0.010}_{-0.002}$	0.0293 ± 0.0009
^{136}Xe	$0.001^{+0.004}_{-0.001}$	0.0177 ± 0.0002
^{150}Nd	$0.013^{+0.007}_{-0.005}$	0.055 ± 0.003

the experimental and calculated NMEs within the given range of V_{0pp} are very small.

In Table IX we give the NMEs for the DD-ME2 interaction, using the optimal value for the isoscalar pairing strength V_{0pp}, in comparison to the values obtained from the experimental data on $2\nu\beta\beta$ decay [80]. The inclusion of $T = 0$ pairing further reduces the NMEs, thus allowing the agreement with the experimental data where previously the calculated NMEs have been too large. However, in many cases the isoscalar pairing reduced the NMEs such that the final result is below the experimental range.

To assess the information about the systematic model dependence of the NMEs for $2\nu\beta\beta$ decay in the REDF framework, we extend our calculations also to the relativistic point-coupling interactions (see Sec. III). In Fig. 11 the NMEs are shown for ^{48}Ca, obtained using point-coupling interactions DD-PC1 and DD-PCX, those with meson-exchange

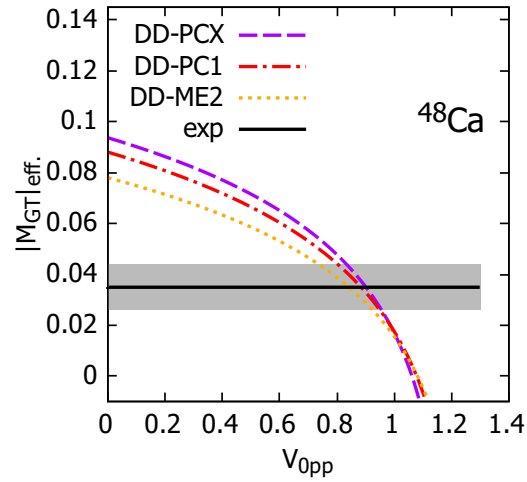

FIG. 11. Comparison of the NMEs for ^{48}Ca using the DD-PC1 and DD-PCX interactions and the value obtained from experimental data [127].

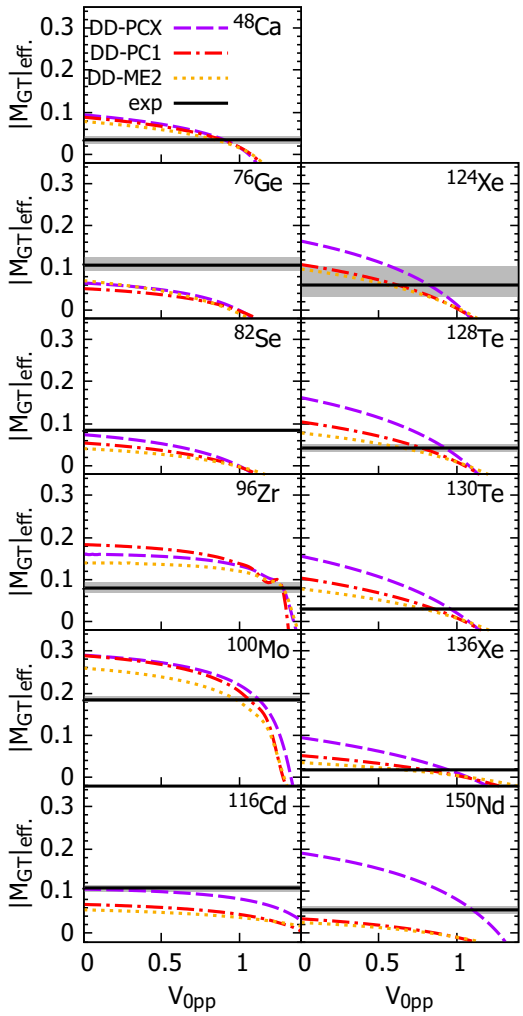

FIG. 12. The dependence of the NMEs on the isoscalar pairing strength V_{0pp} for the $2\nu\beta\beta$ decay for the set of nuclides in the mass range ^{76}Ge–^{150}Nd, for all relativistic interactions employed in this work shown in comparison to the values obtained from the experimental data [127].

interaction DD-ME2, and the NME obtained from the experimental data on $2\nu\beta\beta$ decay [80]. The figure shows the dependence of the NMEs on the $T = 0$ pairing strength V_{0pp}. The results for the two point-coupling interactions display some variations of the NMEs, though not considerable; the NMEs for the DD-PC1 interaction are somewhat lower, e.g., at $V_{0pp} = 0$ the difference in the NMEs for DD-PC1 and DD-PCX interactions is less than ≈0.01. The NMEs for DD-ME interaction show qualitatively the same dependence on V_{0pp}. Similar analysis of the sensitivity of the NMEs on the effective interaction employed is performed for other nuclei of interest, from ^{76}Ge toward ^{128}Te, as shown in Fig. 12. The NMEs for DD-PC1 interaction appear systematically smaller than those of DD-PCX interaction, and their differences provide the insight into the model uncertainties when using different point-coupling interactions. In the case of DD-ME2 interaction, the NMEs are smaller than those of DD-PC1 and DD-PCX interactions, except for ^{76}Ge. The differences depend on the specific nucleus under consideration. For example, for ^{48}Ca the results for the two interactions almost coincide, while for ^{150}Nd considerable differences in the NMEs are obtained.

TABLE X. The same as Table IX but for DD-PC1 and DD-PCX interactions and the corresponding optimal values of the isoscalar pairing strength V_{0pp} given in Table II.

	REDF-QRPA (DD-PC1)	REDF-QRPA (DD-PCX)	Expt. [80]
^{48}Ca	$0.008^{+0.019}_{-0.008}$	$0.024^{+0.016}_{-0.021}$	0.035 ± 0.003
^{76}Ge	$0.003^{+0.021}_{-0.003}$	$0.009^{+0.014}_{-0.009}$	0.106 ± 0.004
^{82}Se	$0.009^{+0.019}_{-0.009}$	$0.005^{+0.014}_{-0.005}$	0.085 ± 0.001
^{96}Zr	$0.148^{+0.016}_{-0.027}$	$0.160^{+0.007}_{-0.011}$	0.080 ± 0.004
^{100}Mo	$0.188^{+0.028}_{-0.049}$	$0.233^{+0.016}_{-0.026}$	0.185 ± 0.002
^{116}Cd	$0.042^{+0.006}_{-0.008}$	$0.087^{+0.005}_{-0.006}$	0.108 ± 0.003
^{124}Xe	$0.034^{+0.036}_{-0.019}$	$0.034^{+0.084}_{-0.034}$	0.059 ± 0.015
^{128}Te	$0.009^{+0.015}_{-0.005}$	$0.012^{+0.015}_{-0.012}$	0.043 ± 0.003
^{130}Te	$0.014^{+0.015}_{-0.013}$	$0.006^{+0.018}_{-0.006}$	0.0293 ± 0.0009
^{136}Xe	$0.007^{+0.006}_{-0.005}$	$0.003^{+0.008}_{-0.003}$	0.0177 ± 0.0002
^{150}Nd	$0.023^{+0.010}_{-0.008}$	$0.066^{+0.019}_{-0.022}$	0.055 ± 0.003

The optimal values for the $T = 0$ pairing strength, obtained for the REDF-QRPA with DD-PC1 and DD-PCX interactions (Table II), can now be employed in description of $2\nu\beta\beta$ decay NMEs. The calculated NMEs are summarized in Table X for DD-PC1 and DD-PCX interactions, respectively, in comparison to the experimental values. Although there are some variations in the NMEs when compared to the experimental data, an overall reasonable qualitative agreement is obtained. This is illustrated in Fig. 13, where we summarize the results of the present study, including the NMEs for $2\nu\beta\beta$ decay obtained using the REDF-QRPA with DD-ME2, DD-PC1, and DD-PCX interactions with the corresponding optimal values of isoscalar pairing strength parameters. For comparison, the NMEs from previous studies are shown, including pn-QRPA implementations by Suhonen [128], Pirinen and Suhonen [1], and Šimkovic *et al.* [84], the IBM [120] and the ISM [112], as well as the experimental result [80]. Clearly, the results of the REDF-QRPA are of comparable quality with those from previous studies, though for most of the nuclei somewhat lower than those determined from the experimental data. In addition, rather than providing just a single NME value, our study provides the insight into systematic uncertainties due to variations in the formulation of the REDF and parametrizations used. Additional uncertainty is accounted for due to the isoscalar pairing strength interaction that is constrained by β-decay half-lives.

The nuclear matrix elements calculated in this work appear rather small compared to previous studies. As already discussed, the isoscalar and isovector pairing strengths are very similar, indicating that the spin-isospin SU(4) symmetry is softly broken. Weak breaking of the SU(4) symmetry could partly explain small NMEs obtained within the REDF-QRPA approach, but even for $V_{0pp} = 0$ the NMEs appear smaller than in other approaches. Another issue is that our treatment did not

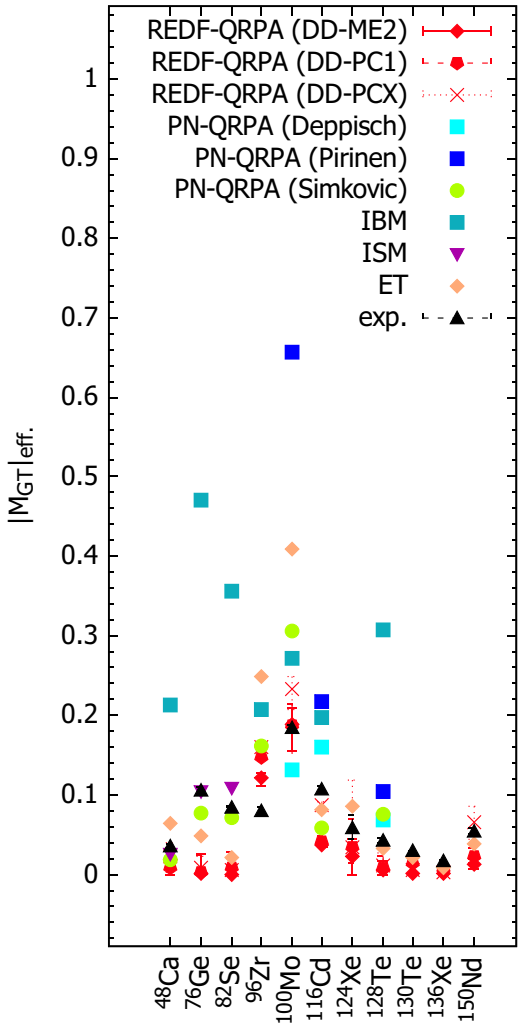

FIG. 13. Summary of the $2\nu\beta\beta$ decay NMEs from the REDF-QRPA with DD-ME2, DD-PC1 and DD-PCX interactions with optimal $T = 0$ pairing together with respective 1σ uncertainties, compared to the calculations based on the pn-QRPA by Deppisch and Suhonen [124], Pirinen and Suhonen [1], and Šimkovic *et al.* [84], IBM [120], ISM [112], and the ET outlined in Ref. [126]. The NMEs from the experimental data [80] are also shown.

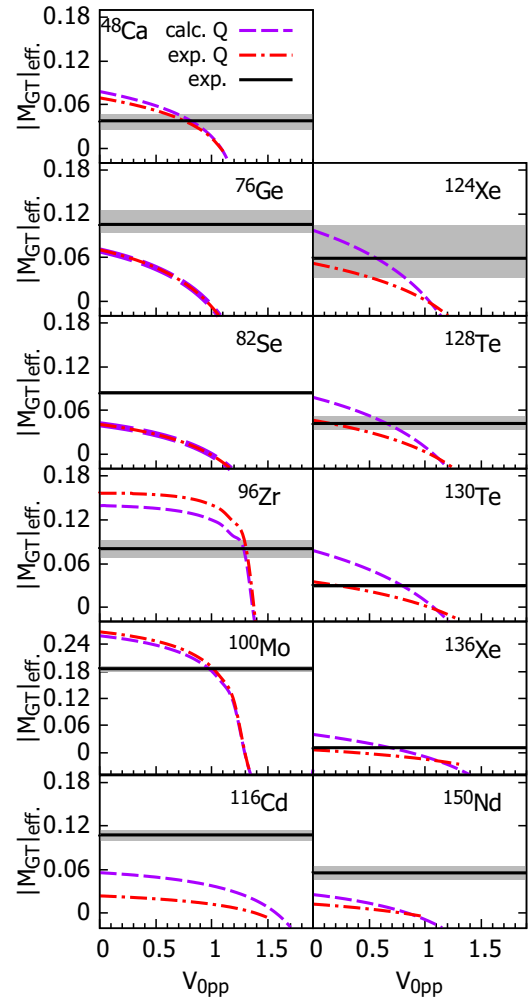

FIG. 14. The NMEs for the DD-ME2 interaction, calculated with the Q values derived self-consistently in the RH-BCS framework, shown next to the NMEs for the same interaction, but with the Q values based on experimental data [130].

include relevant effects going beyond the QRPA, as mentioned in Sec. I.

In order to perform an additional sensitivity check of our calculations we also performed calculations in which Q values derived from the experimental masses have been used. Figure 14 shows the NMEs calculated using the DD-ME2 interaction, both with experimental and calculated Q values. One can observe that the NME results are nearly the same for ^{48}Ca, ^{76}Ge, and ^{82}Se, while for other nuclei the same trend with V_{0pp} is obtained, but some differences can be observed. In several cases the NMEs become smaller when using experimental Q values instead of calculated ones. Thus, the choice of Q value does not provide a solution to the problem of small NME values, except for ^{96}Zr. Whether the $2\nu\beta\beta$ NMEs could be increased by an appropriate treatment of the effects we could not include in the current work is an interesting perspective for the further research. For example, in Ref. [129] the structure of ^{76}Ge and ^{76}Se was studied with Gogny functionals, indicating that the comparison with the experimental data could only be obtained when triaxial shapes have been included, and these are precisely the nuclei for which we obtain the NMEs that diverge the most from experimental results. Also in the present study the systematic uncertainty due to implementation of three different relativistic interactions is considerably larger than the experimental uncertainty. Therefore, further investigations and improvements of the theory frameworks are necessary in order to reduce the theoretical uncertainty obtained from our, but also from other, studies.

V. CONCLUSION

In this work a theory framework is established for the study of $2\nu\beta\beta$ decay nuclear matrix elements based on the relativistic nuclear energy functional. Model calculations include two different formulations of the effective interactions, density-dependent meson-exchange and point-coupling inter-

actions, and three parametrizations (DD-ME2, DD-PC1, and DD-PCX) are employed in order to assess the information on the systematic uncertainties on the NMEs in the relativistic framework. The ground states of nuclei involved in the decay are calculated within the relativistic Hartree-BCS model, while nuclear transitions in the $2\nu\beta\beta$ decay are described using the REDF-QRPA. In addition to the isovector pairing correlations taken into account in the ground-state calculations within the RH-BCS model, the isoscalar pairing channel has also been included in the residual REDF-QRPA interaction, and its optimal values of the strength parameter V_{0pp} are constrained by the experimental data on β-decay half-lives, in order to allow predictions in double-β decay studies.

We calculated the NMEs for a set of nuclei that undergo $2\nu\beta\beta$ decay: ^{48}Ca, ^{76}Ge, ^{82}Se, ^{96}Zr, ^{100}Mo, ^{116}Cd, ^{128}Te, ^{130}Te, ^{124}Xe, ^{136}Xe, and ^{150}Nd. The dependence of the NMEs on the isoscalar pairing strength V_{0pp} was investigated at the limit $V_{0pp} = 0$ and using optimal V_{0pp} values. The NMEs from the REDF-QRPA provide an improvement over the interacting boson model, being closer to the values of the NMEs obtained from the experimental data. However, when compared to the nonrelativistic pn-QRPA, interacting shell model, or effective theory, the NMEs from the present study for most of studied nuclei, with a few exceptions, are rather small. While for some studied nuclei the NMEs are already below experimental ones in the $V_{0pp} = 0$ limit, for several nuclei at this limit the NMEs are above experimental values, but when introducing the optimal value of V_{0pp}, the NMEs become rather low. It was shown that different treatment of the Q-value calculation for most of the studied nuclei could not increase the NMEs, and further studies of additional effects are required to resolve this question. Rather than providing just a single NME value like most of the previous studies, our work provides insight into the systematic uncertainties due to different formulations of the REDF and parametrizations used. Additional uncertainty is accounted for due to the isoscalar pairing strength interaction that is constrained by β-decay half-lives.

This work provides an important benchmark for the future applications of the relativistic framework in studies of neutrinoless double-β decay. However, we note that the present study represents our first study of double-β decays in the relativistic framework, and some effects have not been considered, e.g., nuclear deformation, symmetry restoration, configuration mixing, etc. Future improvements of the REDF-based theory framework, in particular the ongoing development of the deformed REDF-QRPA for the functionals used in this work, will allow additional improvements in modeling nuclear double-β decays.

ACKNOWLEDGMENTS

We thank Deni Vale for support regarding the REDF-QRPA and useful discussions, and Jenni Kotila for discussion on the phase space factors for double-β decays. This work is supported by the QuantiXLie Centre of Excellence, a project co-financed by the Croatian Government and European Union through the European Regional Development Fund, the Competitiveness and Cohesion Operational Programme (KK.01.1.1.01.0004).

[1] P. Pirinen and J. Suhonen, Phys. Rev. C **91**, 054309 (2015).
[2] J. Engel and J. Menéndez, Rep. Prog. Phys. **80**, 046301 (2017).
[3] C. F. Jiao, M. Horoi, and A. Neacsu, Phys. Rev. C **98**, 064324 (2018).
[4] W. Haxton and G. Stephenson, Prog. Part. Nucl. Phys. **12**, 409 (1984).
[5] S. M. Bilenky and C. Giunti, Int. J. Mod. Phys. A **30**, 1530001 (2015).
[6] A. Faessler and F. Simkovic, J. Phys. G: Nucl. Part. Phys. **24**, 2139 (1998).
[7] M. T. Mustonen and J. Engel, Phys. Rev. C **87**, 064302 (2013).
[8] A. Staudt, T. Kuo, and H. Klapdor-Kleingrothaus, Phys. Lett. B **242**, 17 (1990).
[9] H. Primakoff and S. P. Rosen, Rep. Prog. Phys. **22**, 121 (1959).
[10] T. Tomoda, Rep. Prog. Phys. **54**, 53 (1991).
[11] J. Suhonen and O. Civitarese, Phys. Rep. **300**, 123 (1998).
[12] S. R. Elliott and P. Vogel, Annu. Rev. Nucl. Part. Sci. **52**, 115 (2002).
[13] F. T. Avignone, S. R. Elliott, and J. Engel, Rev. Mod. Phys. **80**, 481 (2008).
[14] J. D. Vergados, H. Ejiri, and F. Šimkovic, Rep. Prog. Phys. **75**, 106301 (2012).
[15] R. Saakyan, Annu. Rev. Nucl. Part. Sci. **63**, 503 (2013).
[16] J. D. Vergados, H. Ejiri, and F. Šimkovic, Int. J. Mod. Phys. E **25**, 1630007 (2016).
[17] M. J. Dolinski, A. W. Poon, and W. Rodejohann, Annu. Rev. Nucl. Part. Sci. **69**, 219 (2019).
[18] H. Ejiri, J. Suhonen, and K. Zuber, Phys. Rep. **797**, 1 (2019).
[19] J. Suhonen and O. Civitarese, J. Phys. G: Nucl. Part. Phys. **39**, 085105 (2012).
[20] J. Terasaki and Y. Iwata, Phys. Rev. C **100**, 034325 (2019).
[21] H. Ejiri, Front. Phys. **7**, 30 (2019).
[22] F. Ŝimkovic, J. Schwieger, G. Pantis, and A. Faessler, Found. Phys. **27**, 1275 (1997).
[23] F. Šimkovic, A. Faessler, H. Müther, V. Rodin, and M. Stauf, Phys. Rev. C **79**, 055501 (2009).
[24] V. Rodin, A. Faessler, F. Šimkovic, and P. Vogel, Czech. J. Phys. **56**, 495 (2006).
[25] S. Stoica and H. Klapdor-Kleingrothaus, Nucl. Phys. A **694**, 269 (2001).
[26] P. Beneš, F. Šimkovic, A. Faessler, and W. Kamiński, Prog. Part. Nucl. Phys. **57**, 257 (2006).
[27] S. Stoica and H. V. Klapdor-Kleingrothaus, Eur. Phys. J. A **17**, 529 (2003).
[28] T. R. Rodríguez and G. Martínez-Pinedo, Phys. Rev. Lett. **105**, 252503 (2010).
[29] J. Menéndez, T. R. Rodríguez, G. Martínez-Pinedo, and A. Poves, Phys. Rev. C **90**, 024311 (2014).
[30] V. dos S. Ferreira, A. R. Samana, F. Krmpotić, and M. Chiapparini, Phys. Rev. C **101**, 044314 (2020).

[31] E. Caurier, G. Martínez-Pinedo, F. Nowacki, A. Poves, and A. P. Zuker, Rev. Mod. Phys. **77**, 427 (2005).
[32] J. Kostensalo and J. Suhonen, Phys. Lett. B **802**, 135192 (2020).
[33] J. Suhonen and J. Kostensalo, Front. Phys. **7**, 29 (2019).
[34] J. Barea and F. Iachello, Phys. Rev. C **79**, 044301 (2009).
[35] B. A. Brown, D. L. Fang, and M. Horoi, J. Phys.: Conf. Ser. **966**, 012017 (2018).
[36] J. Barea, J. Kotila, and F. Iachello, Phys. Rev. C **91**, 034304 (2015).
[37] J. Barea, J. Kotila, and F. Iachello, Phys. Rev. C **87**, 014315 (2013).
[38] C. F. Jiao, J. Engel, and J. D. Holt, Phys. Rev. C **96**, 054310 (2017).
[39] P. K. Rath, A. Kumar, R. Chandra, R. Gautam, P. K. Raina, and B. M. Dixit, Int. J. Mod. Phys. E **28**, 1950096 (2019).
[40] J. Kotila, J. Suhonen, and D. S. Delion, J. Phys. G: Nucl. Part. Phys. **37**, 015101 (2010).
[41] F. Simkovic, G. Pantis, and A. Faessler, Yad. Fiz. **61**, 1318 (1998) [Phys. At. Nucl. **61**, 1218 (1998)].
[42] S. Ünlü, N. Çakmak, and C. Selam, Nucl. Phys. A **970**, 379 (2018).
[43] J. Suhonen, Nucl. Phys. A **86463** (2011).
[44] P. Vogel and M. R. Zirnbauer, Phys. Rev. Lett. **57**, 3148 (1986).
[45] J. Engel, P. Vogel, and M. R. Zirnbauer, Phys. Rev. C **37**, 731 (1988).
[46] G. Martínez-Pinedo, K. Langanke, and P. Vogel, Nucl. Phys. A **651**, 379 (1999).
[47] S. Frauendorf and A. Macchiavelli, Prog. Part. Nucl. Phys. **78**, 24 (2014).
[48] N. Hinohara and J. Engel, Phys. Rev. C **90**, 031301(R) (2014).
[49] J. Menéndez, N. Hinohara, J. Engel, G. Martínez-Pinedo, and T. R. Rodríguez, Phys. Rev. C **93**, 014305 (2016).
[50] L. S. Song, J. M. Yao, P. Ring, and J. Meng, Phys. Rev. C **90**, 054309 (2014).
[51] J. M. Yao, L. S. Song, K. Hagino, P. Ring, and J. Meng, Phys. Rev. C **91**, 024316 (2015).
[52] L. S. Song, J. M. Yao, P. Ring, and J. Meng, Phys. Rev. C **95**, 024305 (2017).
[53] N. Paar, D. Vretenar, and P. Ring, Phys. Rev. Lett. **94**, 182501 (2005).
[54] N. Paar, Y. F. Niu, D. Vretenar, and J. Meng, Phys. Rev. Lett. **103**, 032502 (2009).
[55] Y. F. Niu, Z. M. Niu, N. Paar, D. Vretenar, G. H. Wang, J. S. Bai, and J. Meng, Phys. Rev. C **88**, 034308 (2013).
[56] Y. Niu, N. Paar, D. Vretenar, and J. Meng, Phys. Lett. B **681**, 315 (2009).
[57] E. Khan, N. Paar, and D. Vretenar, Phys. Rev. C **84**, 051301(R) (2011).
[58] E. Yüksel, N. Paar, G. Colò, E. Khan, and Y. F. Niu, Phys. Rev. C **101**, 044305 (2020).
[59] A. R. Samana, F. Krmpotić, N. Paar, and C. A. Bertulani, Phys. Rev. C **83**, 024303 (2011).
[60] A. F. Fantina, E. Khan, G. Colò, N. Paar, and D. Vretenar, Phys. Rev. C **86**, 035805 (2012).
[61] D. Vale, T. Rauscher, and N. Paar, J. Cosmol. Astropart. Phys.02 (2016) 007.
[62] J. Petković, T. Marketin, G. Martínez-Pinedo, and N. Paar, J. Phys. G: Nucl. Part. Phys. **46**, 085103 (2019).
[63] X. Roca-Maza and N. Paar, Prog. Part. Nucl. Phys. **101**, 96 (2018).
[64] C. Mondal, B. K. Agrawal, M. Centelles, G. Colò, X. Roca-Maza, N. Paar, X. Viñas, S. K. Singh, and S. K. Patra, Phys. Rev. C **93**, 064303 (2016).
[65] N. Paar, C. C. Moustakidis, T. Marketin, D. Vretenar, and G. A. Lalazissis, Phys. Rev. C **90**, 011304(R) (2014).
[66] J. Dobaczewski, W. Nazarewicz, and P.-G. Reinhard, J. Phys. G: Nucl. Part. Phys. **41**, 074001 (2014).
[67] N. Paar, T. Nikšić, D. Vretenar, and P. Ring, Phys. Rev. C **69**, 054303 (2004).
[68] D. Vale, Y. F. Niu, and N. Paar, Phys. Rev. C **103**, 064307 (2021).
[69] A. Ravlić, Y. F. Niu, T. Nikšić, N. Paar, and P. Ring, Phys. Rev. C **104**, 064302 (2021).
[70] D.-L. Fang, A. Faessler, V. Rodin, and F. Simkovic, Phys. Rev. C **83**, 034320 (2011).
[71] J. Hyvärinen and J. Suhonen, Adv. High Energy Phys. **2016**, 4714829 (2016).
[72] D. S. Delion, A. Dumitrescu, and J. Suhonen, Phys. Rev. C **100**, 024331 (2019).
[73] D.-L. Fang, A. Faessler, and F. Šimkovic, Phys. Rev. C **97**, 045503 (2018).
[74] A. A. Raduta and C. M. Raduta, J. Phys.: Conf. Ser. **413**, 012014 (2013).
[75] F. Šimkovic, R. Dvornický, D. Štefánik, and A. Faessler, Phys. Rev. C **97**, 034315 (2018).
[76] L. M. Robledo, T. R. Rodríguez, and R. R. Rodríguez-Guzmán, J. Phys. G: Nucl. Part. Phys. **46**, 013001 (2019).
[77] F. Šimkovic, V. Rodin, A. Faessler, and P. Vogel, Phys. Rev. C **87**, 045501 (2013).
[78] S. Stoica and M. Mirea, Front. Phys. **7**, 12 (2019).
[79] J. Suhonen, *From Nucleons to Nucleus*, Theoretical and Mathematical Physics (Springer, Berlin, 2007)
[80] A. Barabash, Nucl. Phys. A **935**, 52 (2015).
[81] T. Marketin, L. Huther, and G. Martínez-Pinedo, Phys. Rev. C **93**, 025805 (2016).
[82] A. Ravlić, E. Yüksel, Y. F. Niu, and N. Paar, Phys. Rev. C **104**, 054318 (2021).
[83] A. Ravlić, E. Yüksel, Y. F. Niu, G. Colò, E. Khan, and N. Paar, Phys. Rev. C **102**, 065804 (2020).
[84] F. Šimkovic, A. Smetana, and P. Vogel, Phys. Rev. C **98**, 064325 (2018).
[85] L. de Oliveira, A. R. Samana, F. Krmpotic, A. E. Mariano, and C. A. Barbero, J. Phys.: Conf. Ser. **630**, 012048 (2015).
[86] P. Vogel, J. Phys. G: Nucl. Part. Phys. **39**, 124002 (2012).
[87] M. Aunola and J. Suhonen, Nucl. Phys. A **602**, 133 (1996).
[88] T. Nikšić, N. Paar, D. Vretenar, and P. Ring, Comput. Phys. Commun. **185**, 1808 (2014).
[89] W. Kohn and L. J. Sham, Phys. Rev. **140**, A1133 (1965).
[90] W. Kohn, Rev. Mod. Phys. **71**, 1253 (1999).
[91] G. A. Lalazissis, T. Nikšić, D. Vretenar, and P. Ring, Phys. Rev. C **71**, 024312 (2005).
[92] F. Hofmann, C. M. Keil, and H. Lenske, Phys. Rev. C **64**, 034314 (2001).
[93] S. Typel and H. Wolter, Nucl. Phys. A **656**, 331 (1999).
[94] C. Fuchs, H. Lenske, and H. H. Wolter, Phys. Rev. C **52**, 3043 (1995).
[95] N. Paar, D. Vretenar, E. Khan, and G. Colò, Rep. Prog. Phys. **70**, R02 (2007).

[96] N. Paar, T. Marketin, D. Vale, and D. Vretenar, Int. J. Mod. Phys. E **24**, 1541004 (2015).
[97] T. Nikšić, D. Vretenar, and P. Ring, Phys. Rev. C **78**, 034318 (2008).
[98] E. Yüksel, T. Marketin, and N. Paar, Phys. Rev. C **99**, 034318 (2019).
[99] P. Bonche, H. Flocard, and P. Heenen, Comput. Phys. Commun. **171**, 49 (2005).
[100] P.-G. Reinhard, B. Schuetrumpf, and J. Maruhn, Comput. Phys. Commun. **258**, 107603 (2021).
[101] Y. Tian, Z.-y. Ma, and P. Ring, Phys. Rev. C **80**, 024313 (2009).
[102] C. L. Bai, H. Sagawa, G. Colò, Y. Fujita, H. Q. Zhang, X. Z. Zhang, and F. R. Xu, Phys. Rev. C **90**, 054335 (2014).
[103] J. Toivanen and J. Suhonen, Phys. Rev. Lett. **75**, 410 (1995).
[104] N. Paar, P. Ring, T. Nikšić, and D. Vretenar, Phys. Rev. C **67**, 034312 (2003).
[105] I. Daoutidis and P. Ring, Phys. Rev. C **83**, 044303 (2011).
[106] T. Nikšić, N. Kralj, T. Tutiš, D. Vretenar, and P. Ring, Phys. Rev. C **88**, 044327 (2013).
[107] Y. Tian, Z.-y. Ma, and P. Ring, Phys. Rev. C **79**, 064301 (2009).
[108] Z. Niu, Y. Niu, H. Liang, W. Long, T. Nikšić, D. Vretenar, and J. Meng, Phys. Lett. B **723**, 172 (2013).
[109] E. M. de Guerra, O. Moreno, P. Sarriguren, and M. Ramon, J. Phys.: Conf. Ser. **366**, 012011 (2012).
[110] F. Simkovic, P. Domin, and S. V. Semenov, J. Phys. G: Nucl. Part. Phys. **27**, 2233 (2001).
[111] O. Azzolini, J. W. Beeman, F. Bellini, M. Beretta, M. Biassoni, C. Brofferio, C. Bucci, S. Capelli, L. Cardani, P. Carniti, N. Casali, D. Chiesa, M. Clemenza, O. Cremonesi, A. Cruciani, I. Dafinei, S. Di Domizio, F. Ferroni, L. Gironi, A. Giuliani *et al.*, Phys. Rev. Lett. **123**, 262501 (2019).
[112] L. Coraggio, L. De Angelis, T. Fukui, A. Gargano, N. Itaco, and F. Nowacki, Phys. Rev. C **100**, 014316 (2019).
[113] A. Gando, Y. Gando, T. Hachiya, M. Ha Minh, S. Hayashida, Y. Honda, K. Hosokawa, H. Ikeda, K. Inoue, K. Ishidoshiro, Y. Kamei, K. Kamizawa, T. Kinoshita, M. Koga, S. Matsuda, T. Mitsui, K. Nakamura, A. Ono, N. Ota, S. Otsuka *et al.* (KamLAND-Zen Collaboration), Phys. Rev. Lett. **122**, 192501 (2019).
[114] A. Barabash, Phys. Procedia **74**, 416 (2015).
[115] N. Shimizu, J. Menéndez, and K. Yako, Phys. Rev. Lett. **120**, 142502 (2018).
[116] Fedor Šimkovic, A. Faessler, V. Rodin, P. Vogel, and J. Engel, Phys. Rev. C **77**, 045503 (2008).
[117] J. Menéndez, A. Poves, E. Caurier, and F. Nowacki, Nucl. Phys. A **818**, 139 (2009).
[118] K. Yako, M. Sasano, K. Miki, H. Sakai, M. Dozono, D. Frekers, M. B. Greenfield, K. Hatanaka, E. Ihara, M. Kato, T. Kawabata, H. Kuboki, Y. Maeda, H. Matsubara, K. Muto, S. Noji, H. Okamura, T. H. Okabe, S. Sakaguchi, Y. Sakemi *et al.*, Phys. Rev. Lett. **103**, 012503 (2009).
[119] Y. F. Niu, G. Colò, and E. Vigezzi, Phys. Rev. C **90**, 054328 (2014).
[120] F. Iachello, J. Barea, and J. Kotila, Nucl. Part. Phys. Proc. **265-266**, 25 (2015).
[121] J. Kotila and F. Iachello, Phys. Rev. C **85**, 034316 (2012).
[122] E. Coello Pérez, J. Menéndez, and A. Schwenk, Phys. Lett. B **797**, 134885 (2019).
[123] E. Caurier, F. Nowacki, and A. Poves, Phys. Lett. B **711**, 62 (2012).
[124] F. F. Deppisch and J. Suhonen, Phys. Rev. C **94**, 055501 (2016).
[125] S. S. M. Wong, *Introductory Nuclear Physics* (Wiley-VCH Verlag GmbH & Co. KGaA, Weinheim, 2004).
[126] E. A. Coello Pérez, J. Menéndez, and A. Schwenk, Phys. Rev. C **98**, 045501 (2018).
[127] A. Barabash, Universe **6**, 159 (2020).
[128] J. Suhonen, Phys. Lett. B **607**, 87 (2005).
[129] T. R. Rodríguez, J. Phys. G: Nucl. Part. Phys. **44**, 034002 (2017).
[130] M. Wang, W. Huang, F. Kondev, G. Audi, and S. Naimi, Chin. Phys. C **45**, 030003 (2021).